A facile recycling and regeneration process for spent LiFePO$_4$ batteries

Jian Li[1,2] · Ya Wang[1] · Lihua Wang[1] · Bin Liu[1] · Hongming Zhou[1,2]

Abstract

In response to the potential environment pollution and energy waste caused by the increasing spent lithium iron phosphate batteries (LFPs), many recycling methods have been developed. Among previous studies, the physical recycling method has attracted numerous attention due to its uncomplicated process and high efficiency. This work provides a regeneration mechanism of that the organic carbon layer is in situ coated on the surface of LiFePO$_4$ particles by the decomposition of binder so that improves the conductivity and rate capability. When serving as cathode material for lithium ion battery, the 3 h-regenerated lithium iron phosphate battery delivers an excellent electrochemical performance which shows a discharge specific capacity of 151.55 mAh g^{-1} at 0.2C and delivers a discharge capacity of 120.44 mAh g^{-1} even at 10C compared with pristine spent LFPs. It delivers a discharge capacity of 124.35 mAh g^{-1} in first cycle and maintains 103.12 mAh g^{-1} with a high capacity retention rate of 82.93% after 2000 cycles at 0.5C through 18,650 battery testing. Meaningfully, a facile and sustainable regeneration process has been demonstrated to re-synthesize LiFePO$_4$ from spent LFPs by our study which can be reused as cathode materials for lithium-ion batteries, indicating an economical and facile method to recycle spent LiFePO$_4$ materials in large scale.

1 Introduction

Lithium iron phosphate (LiFePO$_4$, LFP) batteries are widely used in electric vehicles (EVs) and hybrid electric vehicles (HEVs) due to its long term cycle performance and high security in recent years [1–3]. In general, the original structure and content of the electrode material changes and results in capacity fading after using for a long time. Considering the more LiFePO$_4$ batteries used in the market of EVs and HEVs, meaning the more spent batteries. The recovery and reuse of key components in LiFePO$_4$/C batteries and the spent LiFePO$_4$/C batteries have attracted widely attention [4, 5]. Therefore, it is urgent to develop an efficient way to reuse spent LiFePO$_4$ cathode materials for the potential environmental protection and energy waste issues.

Conventional recycling methods frequently recovering precious metals from spent cathode materials and then reusing them on the cathode materials such as LiCoO$_2$, LiMn$_2$O$_4$ or their mixtures [6–8]. At present, there are two main methods for recovery and reuse of cathode materials in spent LiFePO$_4$/C batteries: physical recycling and hydrometallurgical recycling [3, 9–12]. These two methods have their own merits, hydrometallurgical recovery processes can achieve high purity of lithium salts, iron salts and phosphates, physical recycling is facile and low cost. This work is dedicated to finding a green and efficient process to relieve the pressure on recycling so focus on the physical restoration.

The preparation of LiFePO$_4$/C materials in physical recycling process in addition to increasing the proper Li, Fe, P, C and other modifiers [13–18], a suitable sintering process is especially important. According to the principle of physical repairing materials, the general steps about physical repairing of spent LiFePO$_4$/C materials: without destroying the original cladding layer and crystal structure of LiFePO$_4$/C, replenishing the missing elements and calcining under high temperature and cooling so that directly repairing the LiFePO$_4$/C material. Similarly, the calcination temperature plays a crucial role in the synthesis of LiFePO$_4$/C materials [19, 20]. Studies have been reported that when the calcination temperature is higher than 800 °C, LiFePO$_4$ materials tend to decompose into impurities such as LiFe(P$_2$O$_7$), Fe$_x$P, Li$_3$PO$_4$ and P$_2$O$_5$. These impurities not only diminish the purity of the material, but also affect the electrochemical

✉ Hongming Zhou
  zhouhongming@csu.edu.cn

1 School of Materials Science and Engineering, Central South University, Changsha 410083, Hunan, China

2 Hunan Zhengyuan Institute for Energy Storage Materials and Devices, Changsha 410083, Hunan, China

properties (such as reducing the specific capacity of the material, increasing self-discharge). It is disadvantageous for the formation and stability about the crystal structure of $LiFePO_4$ when the calcination temperature is lower than 500 °C [21, 22]. Therefore, the synthesis temperature of the $LiFePO_4$/C material is usually selected from 500 to 750 °C. Li et al. [23] investigated direct regeneration procedure of recycled cathode material mixture from 600 to 800 °C with Li_2CO_3 and at 650 °C displayed excellent electrochemical performances. Chen et al. [24] also proved that cathode powders calcined at 650 °C displayed good electrochemical properties. Song et al. [25] investigated mechanochemical activation mechanisms and about 93.05% Fe and 82.55% Li could be recovered as $FePO_4 \cdot 2H_2O$ and Li_3PO_4 in the mechanochemical activation process. They all have detailed research on how calcination temperature repairs spent cathode material mixture, but the role played by calcination time is not discussed in detail.

In this paper, the spent cathode material mixture with Li_2CO_3 uniformly ball-milling for 6 h and calcining for different time at 700 °C after the element content analysis of Li, Fe and P. A facile and sustainable physical direct regeneration method was studied to repair spent $LiFePO_4$/C without using acid, alkali solution or precipitant, alleviating the high cost of recycling. It could be an ideal of calcination process for spent $LiFePO_4$/C materials due to facile device, less process and higher economic value. Surprisingly, the regenerated material as cathode assembled into a 18,650 battery exhibits superb cycle stability (124.35 mAh g^{-1} in the first cycle and maintains 103.12 mAh g^{-1} after 2000 cycles at 0.5C). In addition, we investigate the crystal structure, morphology of the spent $LiFePO_4$ material and regenerated samples. Therefore, the investigation of physical direct regeneration procedure of recycled cathode material mixtures is valuable for designing and developing advanced recycling process.

2 Experimental

2.1 Cathode material regeneration

Spent soft-pack $LiFePO_4$/C batteries used in this work were from Zhengyuan Research Institute in Hunan Province. In a dry environment, using a pair of scissors to disassemble the batteries, removing the core package, and then separating the spent $LiFePO_4$/C material from the core package. Washing three times by DMC solution, and drying it under 80 °C for 12 h. The separated cathode materials were smashed by a pulverizer, and the aluminum powder was filtered by a sifter to obtain the recovered cathode material mixture. The proportion of element composition in spent $LiFePO_4$ materials detected by Inductively Coupled Plasma Optical Emission Spectrometer (ICP-OES, Blue, Spectro) is shown in Table 1. Adding an appropriate amount of Li_2CO_3 as Li source to keep that the molar ratio of Li to Fe in the material was 1:1. The Li_2CO_3 and cathode material mixture ball milled uniformly and dried for 6 h (Fig. 1). Recycled cathode material mixtures were further directly regenerated at 700 °C for 2 h, 3 h, 4 h, 5 h labeled as 2h-RLFP, 3h-RLFP, 4h-RLFP and 5h-RLFP respectively in high purity N_2 atmosphere.

2.2 Batteries assembly

Regenerated cathode material mixture as active substance, poly (vinyl difluoride) (PVDF) as binder and conductive Super-P in N-methyl-2-pyrrolidinon (NMP) at a weight ratio of 8:1:1. New button batteries were assembled in an argon-filled glove box (Mbraunlab Master130, Germany). Metallic lithium foils were used as counter electrodes and Celgard @ 2325 were used as separators. The electrolyte was 1 M $LiPF_6$ dissolved in a mixture of dimethyl carbonate (DMC), diethyl carbonate (DEC) and ethylene carbonate (EC) (1:1:1 by weight).

2.3 Compositional and structural characterization

The elemental composition and concentration in spent/regenerated materials were detected by ICP-OES (Blue, Spectro). Surface configuration and crystal structure of samples were characterized by scanning electron microscope (SEM, Tescan, MIRA 3 LMU), transmission electron microscopy (TEM, Tecnai G2 F20) and X-ray diffraction (XRD, Siemens D 500). The presence of carbon is characterized by Raman spectra (LabRAMHR800).

2.4 Electrochemical test

New button batteries were tested on a multi-channel battery test system (NEWARE). Galvanostatic discharging/charging cycling was performed at several different current densities between cutoff potentials of 2.0–3.8 V. Cyclic voltammetry (CV) at a scan rate of 0.2 mV s^{-1} and electrochemical impedance spectroscopy (EIS) in the frequency range of 10 mHz to 1000 kHz were tested on the CH instrument 660D electrochemical workstation.

Table 1 Chemical composition of Spent-LFP

Element	Li	Fe	P	Al	M (Li:Fe:P)
Spent-LFP (wt%)	4.31	35.12	20.87	0.53	0.97:1:1.06
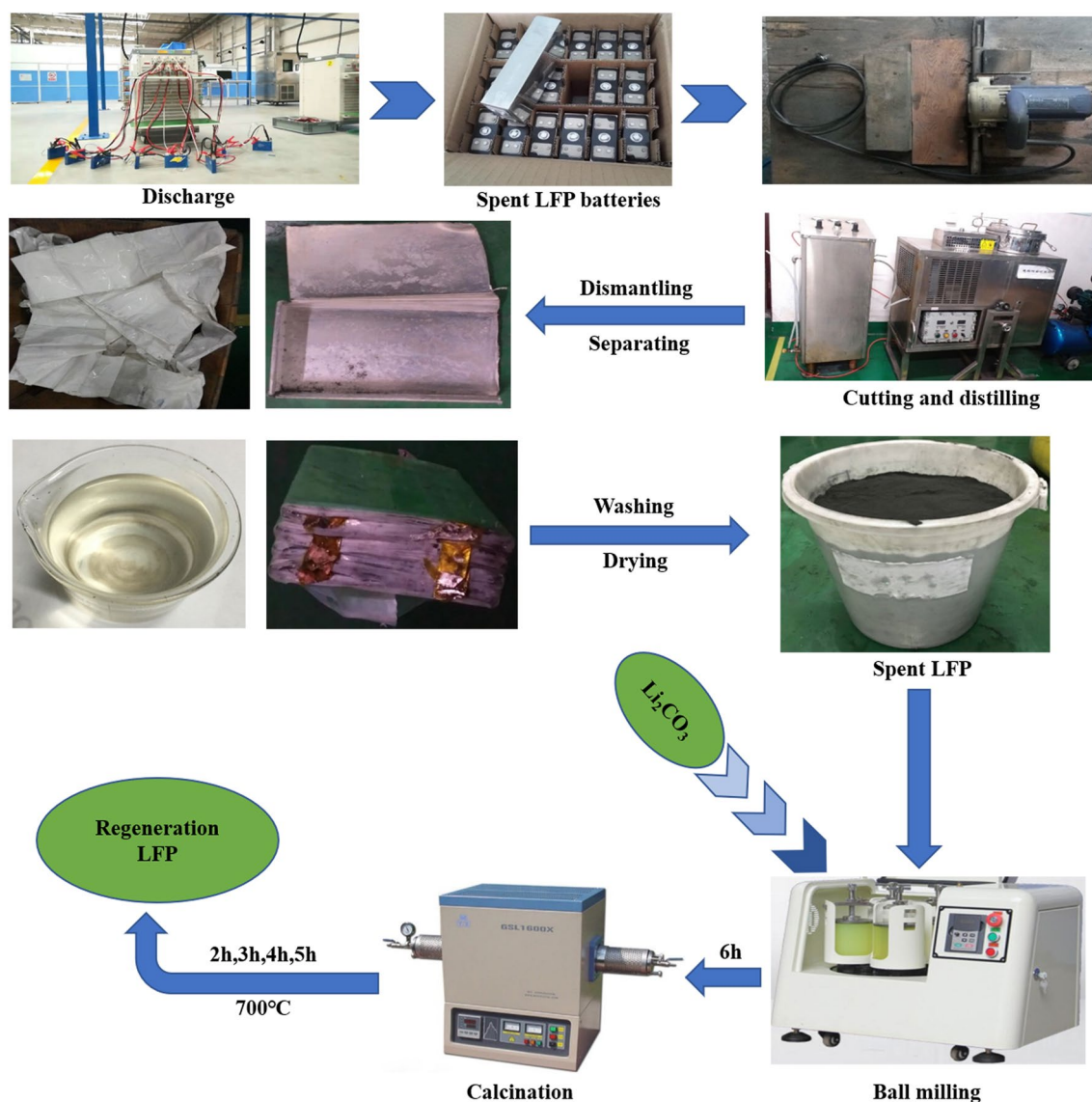
Fig. 1 The flow chart of recycling spent LiFePO$_4$

3 Results and discussion

Figure 2 displays XRD pattern of Li$_2$CO$_3$ and spent LiFePO$_4$ materials to examine their components and phase purity. The characteristic peaks from both spent LFP and Li$_2$CO$_3$ can be indexed to the crystal of LFP (JCPDS 83-2092) and Li$_2$CO$_3$ (87-0729), respectively. Compared with LFP (JCPDS 83-2092), spent LFP emerges three distinct peaks of impurities FePO$_4$, P$_2$O$_5$ and C shown in Fig. 2a. The impurities of FePO$_4$ and P$_2$O$_5$ are caused by the decomposition of some LFP particles [23]. Li sources commonly used for experiment are LiOH, Li$_2$CO$_3$, Li$_2$C$_2$O$_4$, CH$_3$COOLi and CH$_3$(CH$_2$)$_3$Li and in this work using Li$_2$CO$_3$ to synthesize commercial LFP due to its low price. The XRD pattern of Li$_2$CO$_3$ corresponds to the diffraction peak in JCPDS:

87-0729 card shown in Fig. 2b which exhibits good crystallinity and high purity without impurity peak.

Figure 3 shows the XRD pattern of spent LiFePO$_4$ material regenerated in calcination time of 2 h, 3 h, 4 h, 5 h, respectively. Compared with the spent LFP material, the RLFPs have a lower C peak strength. When the calcination time is higher than 3 h, the impurity phase Li$_3$PO$_4$ disappears and when the calcination time is higher than 5 h, the P$_2$O$_5$ impure phase appears in the material and increases gradually because resynthesized LiFePO$_4$ begins to decompose at high regeneration temperature. Therefore, we possess the higher purity RLFP materials when the calcination time is 3 h or 4 h (Fig. 3b). Figure 4 shows the Raman spectroscopy of 2h, 3h, 4h, 5h-RLFP to characterize the surface structure of the regeneration material. Two strong peaks distinctly appear in
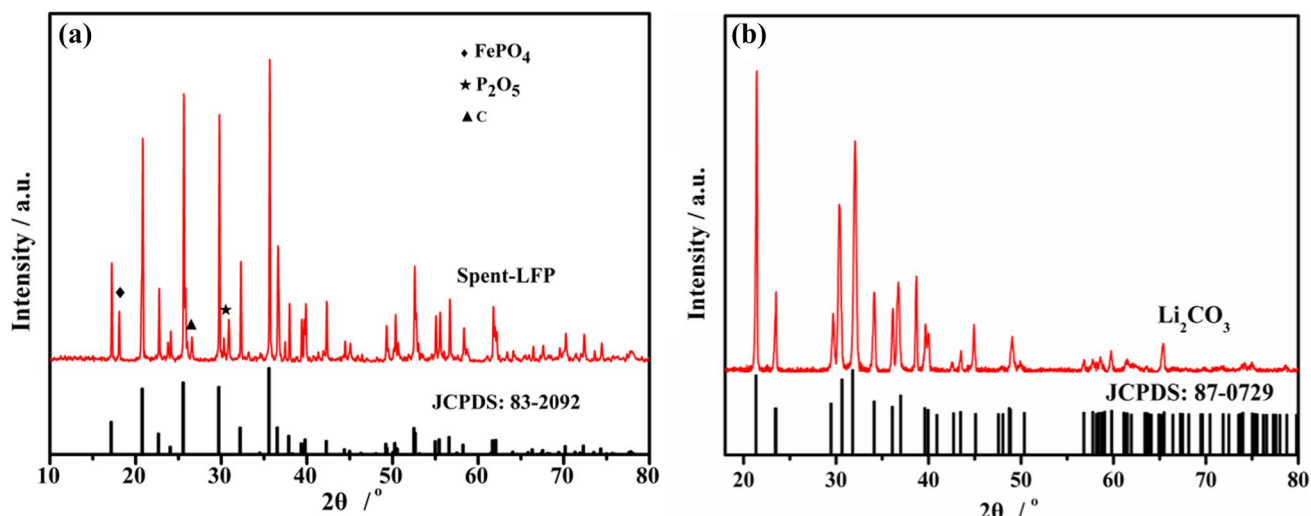
Fig. 2 XRD pattern of **a** Spent-LFP and **b** Li_2CO_3
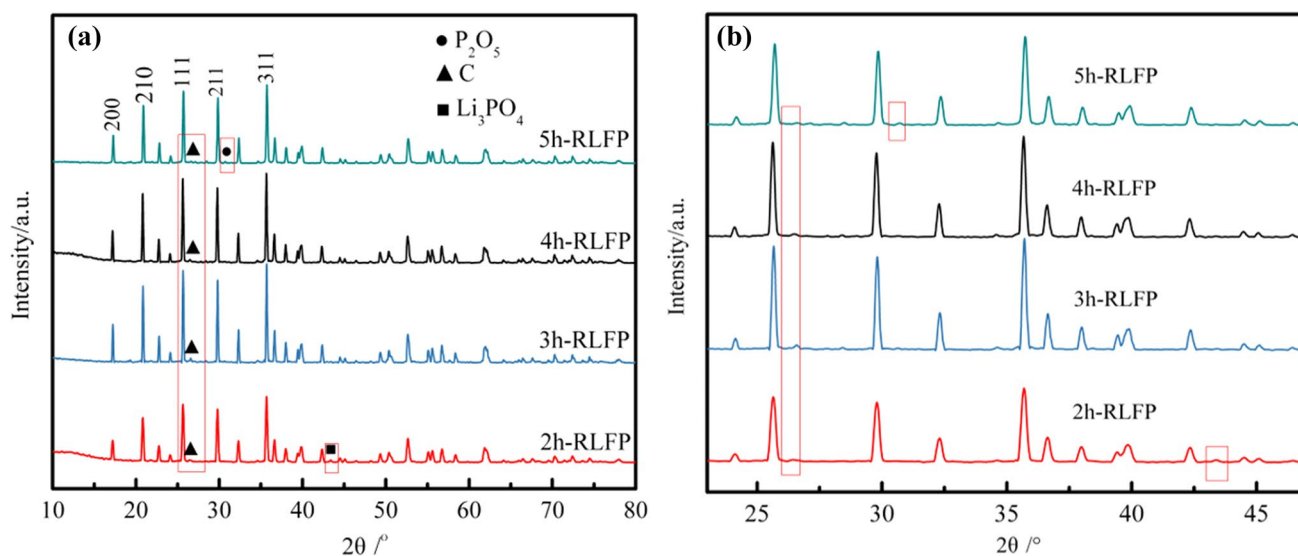
Fig. 3 **a** XRD patterns of 2h, 3h, 4h, 5h-RLFP, **b** is a local enlargement of **a**

1300–1600 cm^{-1}, which correspond to the D and G peaks of carbon. By calculating the ratio of ID/IG, characterizing the ordering degree of carbon materials. When the calcination temperature is 3–5 h, the ordering degree of the material's surface is identical corresponding to the ID/IG of 1.28, 1.10, 1.10 and 1.10 of 2h, 3h, 4h, 5h-RLFP respectively, demonstrating high graphitization and ordering of the 3h-RLFP's surface.

The morphology and particle size of the spent-LFP, 2h, 3h, 4h, 5h-RLFP were examined by SEM. As shown in Fig. 5, the particle size of the RLFP continues to increase with the calcination time extending but accompany some small broken particles. Figure 5a shows that serious agglomeration phenomenon and broken particles due to residual of

PVDF. With the decomposition of residual PVDF binder, the agglomeration phenomenon gets relieved or even disappear. Figure 5b shows that the RLFP particles are not fully grown compared with the RLFP particles shown in Fig. 5c. In addition, the agglomeration of particles is more severe shown in Fig. 5d, e, revealing that the binder may decompose into a substance that is dispersed between the RLFP particle and C particle or among RLFP particles as the calcination time increases. Figure 5c exhibits a superior morphology and spherical RLFP particles with a diameter ranging from 1 to 2 μm.

TEM images are shown in Fig. 6 to further investigate the microstructure of the 3h-RLFP. PVDF as the binder turns into liquid so that wetting the RLFP particles in molten state
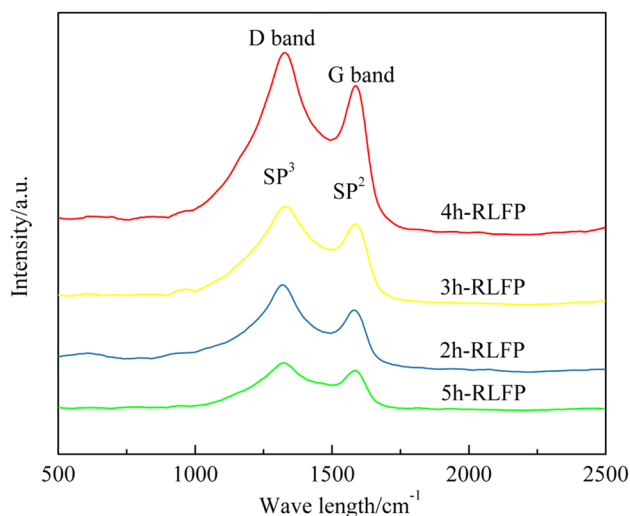
Fig. 4 Raman spectra of 2h, 3h, 4h, 5h-RLFP

by the capillary force after calcination. PVDF is decomposed into the amorphous carbon material as the reaction (1).

$$[C_2H_2F_2]_n \rightarrow nHF\ (gas)\ +nC \tag{1}$$

As shown in Fig. 6a, the selected area reflects the severe structural disorder in spent-LFP particles noticeably. Those defects in the spent samples indicate that spent LFP particles suffer from lattice distortion and cracking during long-term charge and discharge cycling. Incomplete or broken LFP particles are caused by the generation of HF gas. And the amorphous carbon material converges among the RLFP particles for the conformation of a recognizable carbon layer (Fig. 6b). It can be observed from Fig. 6c, d that amorphous carbon materials co-coat the surface of intrinsic RLFP particles or conductive particles gradually, leading to non-uniform thickness of coated layers on the surface of RLFP particles. Figure 6d exhibits unevenly coated layer on the part of the RLFP particle, indicating although the materials can be repaired at 700 °C for 3 h, the generation of HF gas still causes unevenness of the coating. As the calcination time is prolonged, there still has amorphous carbon material deposited on the coating layer of the original carbon-coated RLFP particles and may result in a thicker coating layer shaping to hinder lithium ion insertion/extraction (Fig. 6e).

The charge–discharge curves of 2h, 3h, 4h, 5h-RLFP materials at 0.2C rate in the voltage of 2.0–3.8 V are shown in Fig. 7a, which exhibits a relatively stable charge and discharge voltage platform with voltage differences. The charge and discharge curves of Spent-LFP display a morphology with large polarization, which reflects that spent LiFePO$_4$ materials suffer severe structural defect during long-term utilization [3]. The electrochemical performance of the spent sample is revitalized again via simple physical regeneration assisted heat retreatment and extended regeneration
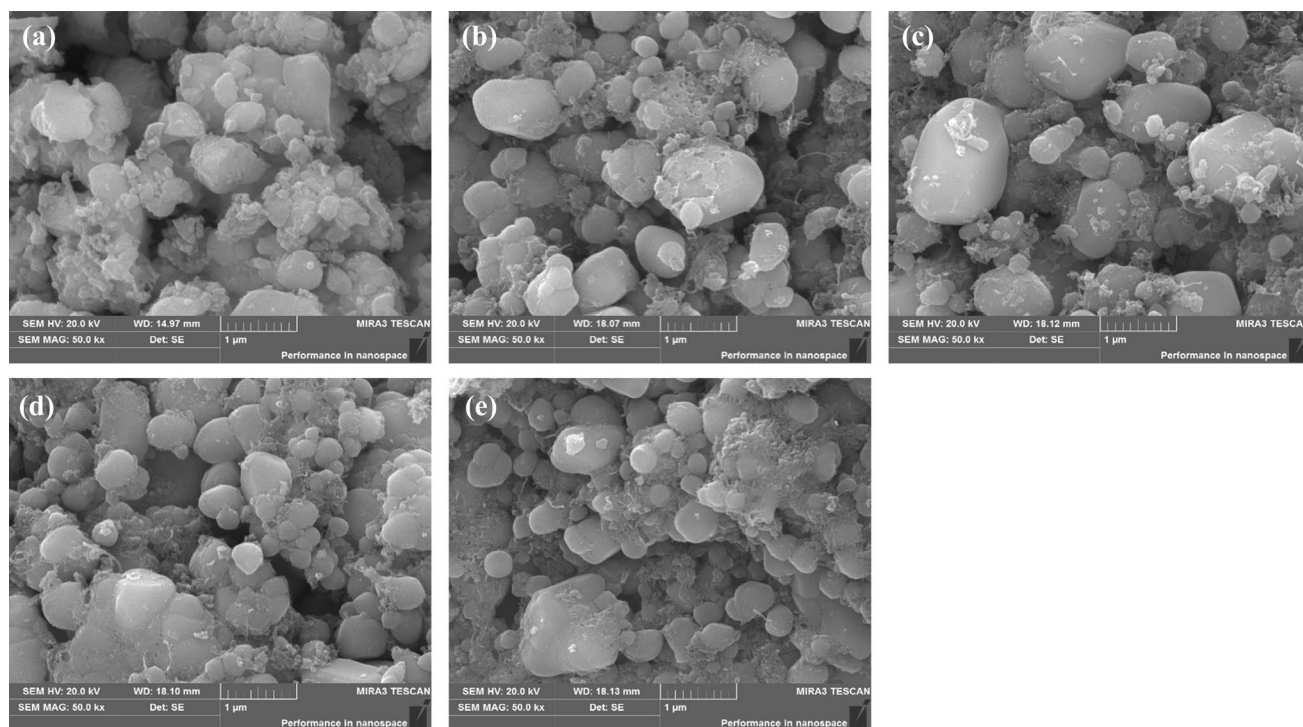
Fig. 5 SEM images of **a** Spent-LFP, **b** 2h-RLFP, **c** 3h-RLFP, **d** 4h-RLFP, **e** 5h-RLFP

Fig. 6 TEM images of **a** Spent-LFP, **b**–**d** 3h-RLFP at different resolutions, **e** Schematic illustration of PVDF decomposes as amorphous carbon in situ coated LiFePO$_4$ particles for further lithium ions migration
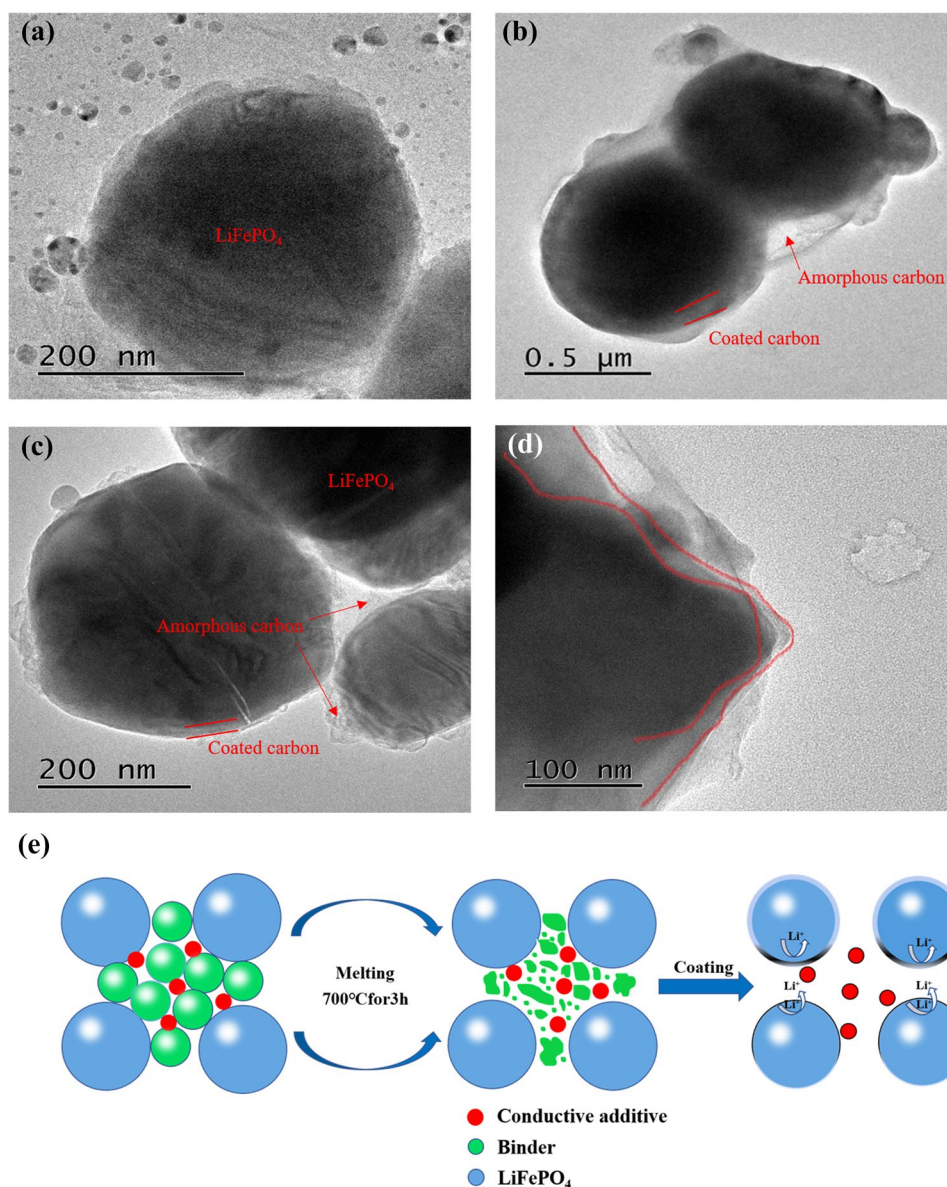
time. The corresponding discharge capacities of the investigated materials at 0.2C rate are 148.49, 151.55, 156.34 and 154.79 mAh g^{-1}, respectively. Among those cathode materials, 3h-RLFP delivers a charge capacity of 160.29 mAh g^{-1} and a discharge capacity of 151.55 mAh g^{-1} at 0.2C with a higher coulomb efficiency of 94.55%. Figure 7b shows the rate capabilities of 2h, 3h, 4h and 5h-RLFP evaluated from 0.2 to 10C then back to 0.2C and five cycles are performed at a given rate, which is convenient in comparison of the discharge capacity for five simples. Compared with Spent LFP, the discharge capacity of RLFPs are greatly promoted at rates from 0.1 to 10C. The 3h-RLFP displays a superior rate performance to the other RLFPs, with the discharge capacities of Spent-LFP, 2h-RLFP, 3h-RLFP, 4h-RLFP and 5h-RLFP presenting as 102.15, 129.22, 132.38, 130.28 and 124.95 mAh g^{-1} at the 5C rate and 97.5, 115.31, 120.44,

117.53 and 112.66 mAh g^{-1} at the 10C rate, respectively. These results collectively illustrate that physical direct regeneration for 3 h at 700 °C is the optimized condition for promoting the electrochemical performance of regenerated LiFePO$_4$/C materials. The capacities of the five samples similar to their initial discharge capacities at the final cycle of 0.1C due to the good electrochemical reversibility and structural stability of phosphor-olivine LiFePO$_4$. The 3h-RLFP exhibits superior cycling performance shown in Fig. 7c, which delivers a discharge capacity of 152.42 mAh g^{-1} in the initial cycle and still remains 148.94 mAh g^{-1} with a high capacity retention rate of 97.71% at 0.5C after 200 cycles compared with Spent-LFP, 2h, 3h, 4h, 5h-RLFP (Table 2).

Figure 8a illustrates the CV profiles of the 2h, 3h, 4h, 5h-RLFP electrodes at a scan rate of 0.2 mV s^{-1} between
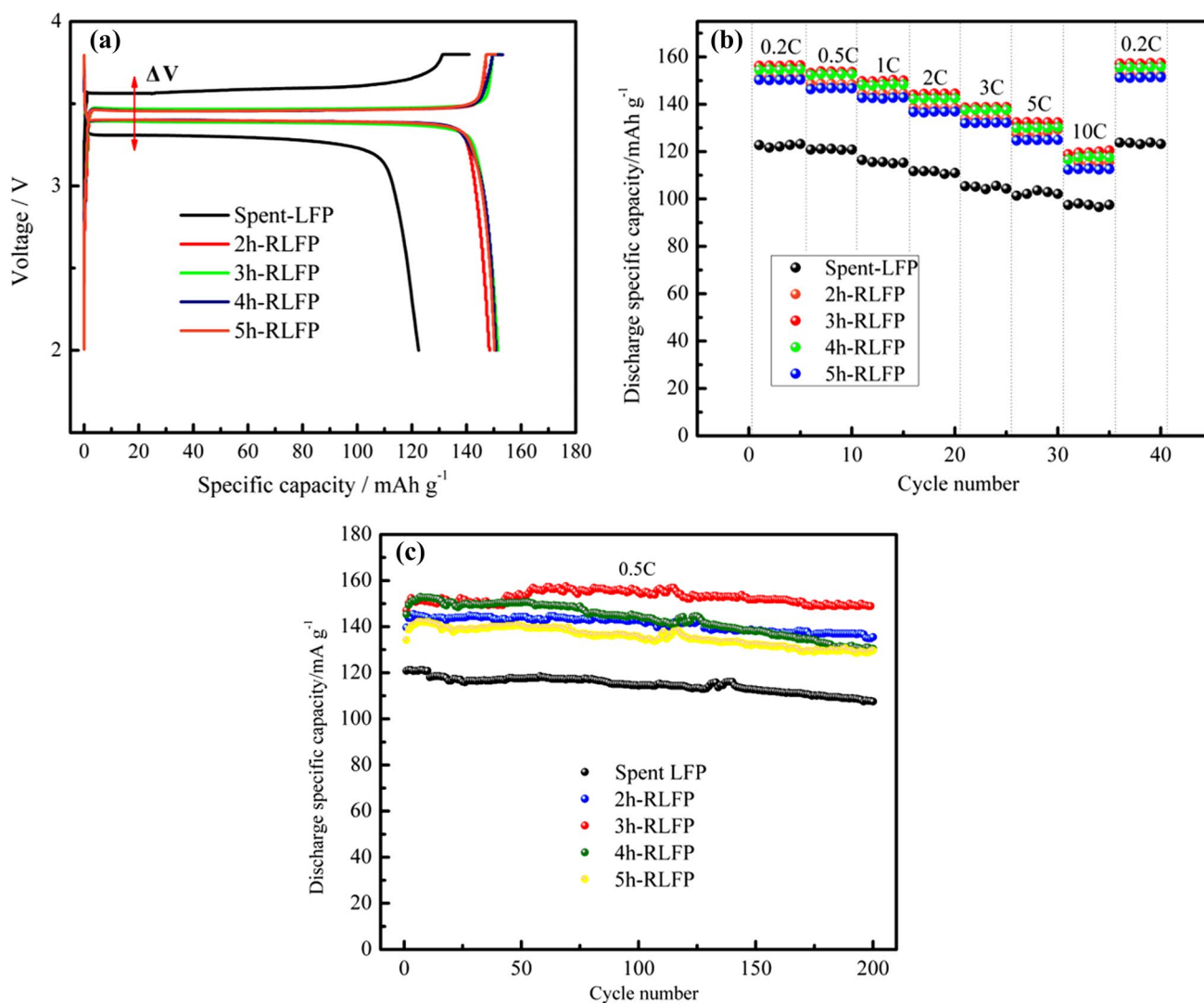
Fig. 7 **a** Charge–discharge curve of Spent-LFP, 2h, 3h, 4h, 5h-RLFP at 0.2C rate, **b** rate capabilities of Spent-LFP, 2h, 3h, 4h, 5h-RLFP in the voltage range of 2–3.8 V, **c** cycling performance of Spent-LFP, 2h, 3h, 4h, 5h-RLFP at 0.5C rate

Table 2 The discharge capacity and capacity retention rate of Spent-LFP, 2h, 3h, 4h, 5h-RLFP

Electrode	Capacity retention rate (%)	Discharge capacity (mAh g⁻¹)	
		1st	200th
Spent-LFP	89.01	120.84	107.56
2h-RLFP	92.70	145.49	134.87
3h-RLFP	97.71	152.42	148.94
4h-RLFP	85.75	152.18	130.50
5h-RLFP	90.70	141.98	128.77

2.0 and 4.5 V which shows a low polarization, symmetric and speculate peak, confirming an excellent reversibility for the RLFPs about lithium ion insertion and extraction. The

oxidation–reduction peak voltage differences of 2h-RLFP, 3h-RLFP, 4h-RLFP and 5h-RLFP are 0.421, 0.353, 0.362 and 0.367 V, respectively. Therefore, the voltage difference of redox peak is the smallest and the electrode polarization is minimum when using 3h-RLFP as cathode. The 3h-RLFP also possesses the largest current of the reduction peak (I = 1.847 mA) and the highest ionic conductivity of lithium ion.

Figure 8b shows the fitting result of electrochemical impedance spectroscopy (EIS) and equivalent circuit diagrams of RLFP materials with the scanning frequency range from 10 mHz to 1000 kHz. The high frequency region of the semicircle denotes charge transfer impedance and the sloped lines in the low frequency region is attributed to the Warburg impedance (W) associated with the solid-state Li-ions diffusion into the electrode materials [26]. R_s refers to
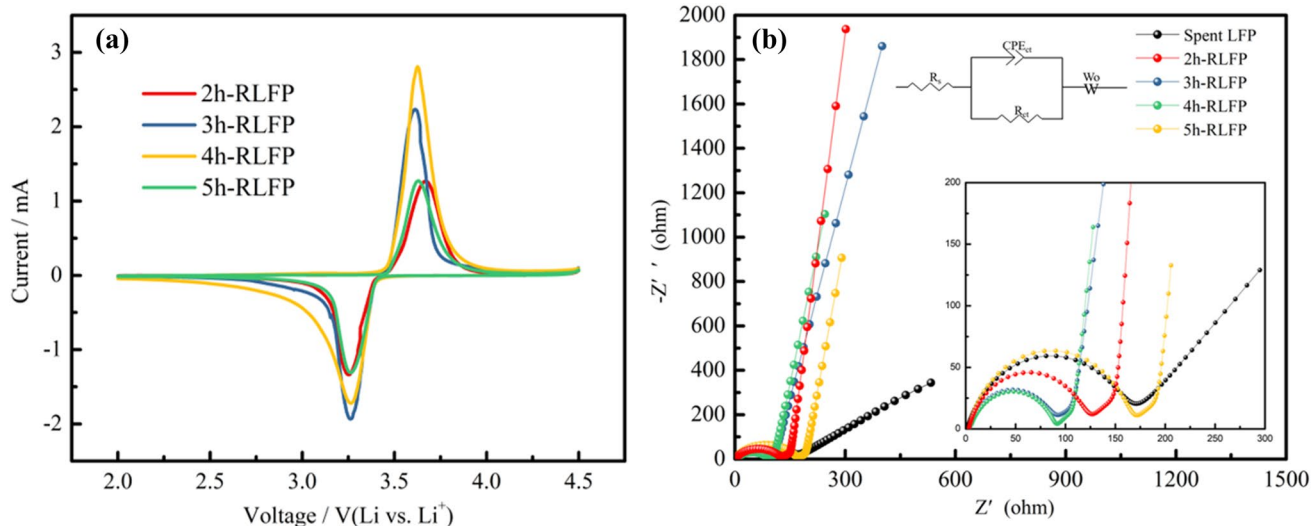
Fig. 8 **a** Cyclic voltammetry curves of 2h, 3h, 4h, 5h-RLFP in the voltage range of 2.0–4.5 V at the scan rate of 0.2 mV s^{-1}, **b** electrochemical impedance spectra (EIS) curves of Spent-LFP, 2h, 3h, 4h, 5h-RLFP in the frequency range from 10 mHz to 1000 kHz with corresponding equivalent circuit

Table 3 Fitting results of various electrodes based on equivalent electric circuit from Fig. 8b

Electrode	Rs (Ω)	Rct (Ω)
Spent-LFP	3.27	153.10
2h-RLFP	3.15	88.21
3h-RLFP	2.92	64.32
4h-RLFP	2.17	73.40
5h-RLFP	1.35	94.80

the uncompensated resistance which might contains particle–particle contact resistance and the resistance between the electrode and the current collector [27]. Table 3 reveals the fitting results of each electrode based on the equivalent circuit in Fig. 8b. One semicircle and one straight line are observed in all regenerated cathode materials, indicating significantly reduced high film impedance [23]. Compare with Spent-LFP, the deteriorated particles internal structure corresponds to the increase of charge transfer impedance (Rct) of regenerated ones. And the 3h-RLFP material possesses slightly deteriorated structure compared to other regenerated samples. Because PVDF in cathode material decomposes to HF gas during high temperature regeneration procedure, which destroys LiFePO$_4$ structure [23]. The changes of EIS curves show that LiFePO$_4$ particles surface after regenerated reasonable time has been effectively repaired due to re-synthesis of LiFePO$_4$. After regenerated for 2 h, HF gas has been released a lot, leading to deteriorated structure and corresponding to a larger Rct. When regenerated than 3 h, the Rct of regenerated ones increases, indicating that the decomposition of PVDF into carbon accumulates in the coating layer which gradually forms an excessively thick layer, thereby increases the lithium ions migration resistance. From 2h-RLFP to 5h-RLFP, the Rs decreases because particles interior is gradually regenerated as the regeneration time increases.

Among those regenerated ones, LiFePO$_4$ particles surface of 3h-RLFP is effectively regenerated because of favorable temperature and moderate time, leading to small Rct and excellent high rate performances at 10 C (Fig. 7b). The charge transfer resistance of the 3h-RLFP is the smallest of 64.32 Ω among those electrodes, indicating that the distinctive in situ carbon-coated structure effectively reduces the barrier for lithium ion transfer at the electrode–electrolyte interface.

18,650 battery was fabricated and tested with the 3h-RLFP as cathode and graphite as anode. Cycling capability of 3h-RLFP in the voltage range of 2.0–3.8 V at the rate of 0.5C during 18,650 battery discharging process is shown in Fig. 9. The 3h-RLFP possesses a superior cycling stability, which delivers a discharge capacity of 124.35 mAh g^{-1} in the first and maintains 103.12 mAh g^{-1} with a high capacity retention rate of 82.93% after 2000 cycles at 0.5C. The promising result brought by 3h-RLFP can be expected to be applied to the cathode of lithium-ion batteries.

4 Conclusion

A facile and sustainable physical-direct regeneration method was researched to recycle spent LiFePO$_4$ batteries in this work. It is demonstrated that the 3h-RLFP not only possesses superb morphology but also has an enhanced electrochemical performance which shows the excellent discharge specific capacity of 151.55 mAh g^{-1} with a high capacity
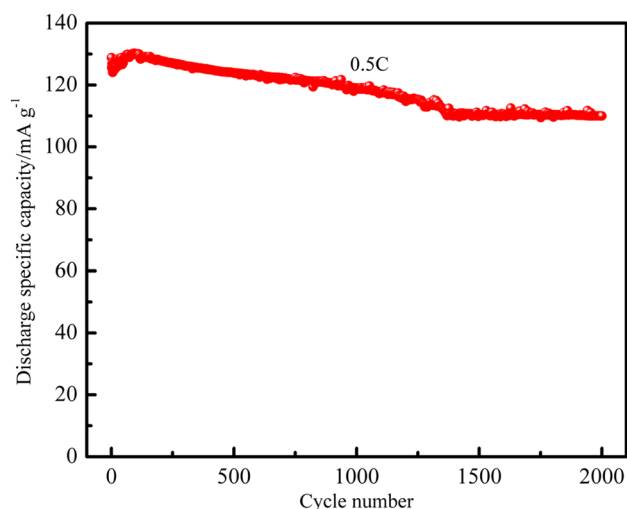
Fig. 9 Cycling performance of 3h-RLFP as cathode in the voltage range of 2.0–3.8 V at the rate of 0.5C by 18,650 battery discharge testing

retention rate of 97.77% at 0.2C rate. In addition, the in situ coated carbonaceous layer improves the conductivity and stimulates a better rate capability with a discharge capacity of 120.44 mAh g^{-1} at a relatively high rate of 10C compared with pristine spent LFP. 18,650 battery testing delivers a discharge capacity of 124.35 mAh g^{-1} in the first cycle and maintains 103.12 mAh g^{-1} with capacity retention rate of 82.93% after 2000 cycles at 0.5C. Overall, the fabrication process of 3h-RLFP can be considered as a facile and large-scale recycling method for lithium-ion batteries.

References

1. C.W. Sun, S. Rajasekhara, J.B. Goodenough, F. Zhou, J. Am. Chem. Soc. **133**, 2132–2135 (2011)
2. A.S. Aricò, P. Bruce, B. Scrosati, J.M. Tarascon, W.V. Schalkwijik, Nat. Mater. **4**, 366–377 (2005)
3. D. Bian, Y. Sun, S. Li et al., Electrochim. Acta **190**, 134–140 (2016)
4. G.Q. Cai, K.Y. Fung, K.M. Ng, Ind. Eng. Chem. Res. **53**, 18245–18259 (2014)
5. T. Georgi-Maschler, B. Friedrich, R. Weyhe, H. Heegn, M. Rutz, J. Power Sources **207**, 173–182 (2012)
6. H.Y. Zou, E. Gratz, D. Apelian, Y. Wang, Green Chem. **15**, 1183–1191 (2013)
7. T. Zhang, Y.Q. He, F.F. Wang, L.H. Ge, X.N. Zhu, H. Li, Waste Manag. **34**, 1051–1058 (2014)
8. Y. Zhang, Y. Zhang, Y. Zhang et al., J. Alloys Compds. **783**, 357–362 (2019)
9. X. Zhang, L. Li, E. Fan, Q. Xue, Y. Bian, F. Wu, R. Chen, Chem. Soc. Rev. **47**(19), 7239–7302 (2018)
10. L. Yang, G. Xi, Y. Xi, Ceram. Int. **41**, 11498–11503 (2015)
11. Q. Sa, E. Gratz, M. He, W. Lu, D. Apelian, Y. Wang, J. Power Sources **282**, 140–145 (2015)
12. P. Meshram, B.D. Pandey, T.R. Mankhand, Chem. Eng. J. **281**, 418–427 (2015)
13. R. Gupta, S. Saha, M. Tomar, V.K. Sachdev, V. Gupta, J. Mater. Sci.: Mater. Electron. **28**(7), 5192–5199 (2017)
14. S.Y. Chung, Y.M. Chiang, Electrochem. Solid-State Lett. **6**(12), A278–A281 (2003)
15. X. Hui, Z. Zhou, Electrochim. Acta **51**(10), 2063–2067 (2006)
16. C.Y. Chiang, H.C. Su, P.J. Wu, H.J. Liu, C.W. Hu, N. Sharma et al., J. Phys. Chem. C **116**(46), 24424–24429 (2012)
17. H. Liu, Q. Cao, L.J. Fu, C. Li, Y.P. Wu, H.Q. Wu, Electrochem. Commun. **8**(10), 1553–1557 (2006)
18. J.F. Ni, H.H. Zhou, J.T. Chen, X.X. Zhang, Mater. Lett. **59**(18), 2361–2365 (2005)
19. F. Feng, R. Lu, C. Zhu, Energies **7**(5), 3004 (2014)
20. Y. Xing, W. He, M. Pecht, K.L. Tsui, Appl. Energy **113**, 106–115 (2014)
21. F. Feng, R. Lu, G. Wei, C. Zhu, Energies **8**(4), 2950 (2015)
22. C. Fleischer, W. Waag, H.-M. Heyn, D.U. Sauer, J. Power Sources **262**, 457–482 (2014)
23. X. Li, J. Zhang, D. Song et al., J. Power Sources **345**, 78–84 (2017)
24. J. Chen, Q. Li, J. Song et al., Green Chem. **18**, 2500–2506 (2016)
25. Y. Yang, X. Zheng, H. Cao et al., ACS Sustain. Chem. Eng. **5**, 9972–9980 (2017)
26. L. Li, A.O. Raji, J.M. Tour, Adv. Mater. **43**, 6298–6302 (2013)
27. S. Yoon, C. Liao, X.-G. Sun, C.A. Bridges, R.R. Unocic, J. Nanda et al., J. Mater. Chem. **22**(11), 4611 (2012)